2022年度　11）SCOSTEP Visiting Scholar (SVS) Program (in ISEE)　目次詳細

2022　11）SCOSTEP Visiting Scholar (SVS) Program in ISEE
List

8 件

＊所属・職名は2023年3月現在
＊Affiliation and Department displayed are current as of March 2023.

(注1)：新型コロナウイルスの影響で中止／Cancelled due to COVID-19
(注2)：中止／Cancelled

研究代表者 Principal Investigator	所属機関* Affiliation	職名* Job title	研究課題名 Project Title	頁 Page	備考 Remarks
Rahul Rathi	Indian Institute of Technology Roorkee, India	graduate-course student	Determination of local geomagnetic index and its correlation with TEC and airglow intensity	308	
Veera Kumar Maheswaran	SASTRA Deemed University, India	graduate-course student	Investigation of latitudinal dependence of medium-scale traveling ionospheric disturbances detected from GNSS TEC data over equatorial regions	309	
Chukwuma Anoruo	University of Nigeria, Nsukka, Nigeria	graduate-course student	Study of TEC variations during geomagnetic storms	311	
Pankaj Kumar Soni	Indian Institute of Geomagnetism, India	graduate-course student	Investigation of flux enhancement and associated changes in pitch angle distributions of radiation belt particles	313	
Nilesh Chauhan	Indian Institute of Geomagnetism, India	graduate-course student	Study of mesospheric bores from middle and high latitude region	316	
Rukundo Wellen	Egypt-Japan University of Science and Technology, Egypt	graduate-course student	Detection of equatorial plasma bubbles (EPBs) using a low-cost 630.0 nm all-sky imager	318	
Adithya H.N. (SVS 2021 Recipient)	Scikraft Education and Engineering Design Pvt. Ltd. India	graduate-course student	Coronal temperature variability from spatially resolved images of the Sun from Hinode/XRT	320	
Onyinye Gift Nwankwo	University of Michigan, USA	graduate-course student	Extensive investigation, comparison and validation of the thermospheric wind observations during geomagnetic quiet and disturbed periods using the data surveys from ground-based equipment and results from model calculations	322	

Small enhancements in the red and green line airglow emissions at sub-auroral latitudes during isolated substorms

Principal Investigator: **Rahul Rathi**

Affiliation: **Indian Institute of Technology Roorkee, India**

Position: **Senior Research Fellow**

As a SCOSTEP visiting scholar (SVS), I worked at Institute for Space-Earth Environmental Research (ISEE) for three months (December 7, 2022, to March 6, 2023) under the supervision of Prof. Kazuo Shiokawa. During this period, I studied the effects of geomagnetic substorms on the ionosphere at sub-auroral latitudes.

The purpose of the study was to investigate the effects of isolated substorms over the sub-auroral latitudes. In order to fulfil this, we used two years (2018-2019) data of Optical Mesosphere Thermosphere Imager (OMTI) installed at Kapuskasing (49.39ºN, 277.81ºE), Canada. We also used ground-based magnetometers, satellite (GOES, ARASE, THEMIS, and SWARM) data. In this study, we identified five substorm events on cloud free nights and investigated their effects on ionospheric red (630.0 nm) and green (557.7 nm) line airglow emissions. Out of the five substorm events, four events showed enhancement in both the red and green line emissions after substorm onset, whereas one event showed enhancement in the red line emission only. As part of this work, we have finalized the figures. Currently, we are investigating the physical mechanisms behind such unique observations and are going to start writing the manuscript.

It was an excellent experience to learn about new datasets, techniques, and concepts at ISEE. During this visit, I gained vast knowledge about future trends, opportunities, and challenges in auroral and sub-auroral latitudes. It will be very beneficial for my ongoing and future research career.

(Form 11-1)

Solar activity dependence for the relationship between nighttime Medium-Scale Traveling Ionospheric Disturbance and Sporadic E-layer activities in summer during 1998-2019 over Japan

Veera Kumar Maheswaran, RF centre for Excellence, Department of ECE, School of Electrical and Electronics Engineering, SASTRA Deemed University, Thanjavur-613401, India, Ph. D Student.

1. Purpose of this study : To understand the solar activity dependence of the medium-scale traveling ionospheric disturbances (MSTIDs) and its coupling with Sporadic-E (Es) layer during summer night of Japan, total electron content (TEC) data obtained from a Global Positioning System (GPS) receiver network and Es parameter can be availed from Ionosonde. Otsuka et al., (2013) studied the seasonal and local time variation of GPS-TEC measured MSTID over Europe. MSTIDs are the wave like structural disturbance in the plasma density in the ionosphere, having with horizontal length of approximately 100 km wavelength with 15 minutes to 1 hour period. MSTID are the plasma manifestation of atmospheric gravity wave (AGW) propagating in the thermosphere in day time. Until late 1990s many techniques are used for observe MSTIDs includes ionosondes, high frequency (HF) radars etc. Late 1990s GPS receiver networks and all-sky airglow imagers are employed for observing two dimensional horizontal structure of MSTID (Saito et al., 1998). Perkins found that there was a spread-F in the F-layer consider to be caused the MSTID in night time (Perkins., 1973). Shiokawa et al., (2003) found that there was an electric field perturbation associated with the night time MSTID called as electrified MSTID (EMSTID). The oscillation of the polarization electric field is reported to play an important role in generating MSTIDs over the midlatitude region. The coupling mechanisms between the neutral atmosphere, ionosphere, and magnetosphere significantly influence the Earth's lower ionosphere and Es-layer. Research findings showed that coupling the E and F regions may intensify the Perkins instability. Otsuka et al., (2021) statistically studied the solar activity dependence of MSTID from 1998-2019 using GPS-TEC over Japan, the growth rate of night time MSTID increases with decreasing solar activity due to the growth rate of Perkins instability. The day time MSTID anticorrelation with the Solar activity and correlated with the secondary AGW under low solar activity condition. These inference motivated that to understand how the Solar activity dependence of night time EMSTID and its coupling with Es- layer during the summer nights.

2. Methodology: In order to reveal solar activity dependence of the connection between MSTID and Es-layer, TEC obtained from a GPS network in Japan and ionosonde data collected at Kokubunji (35.7°N, 139.5°E), Japan between May and August of 1998 and 2019 are analyzed. We have calculated the detrended TEC by subtracting the 1-hour running average from the original TEC data for each satellite and receiver pair to obtain the perturbation TEC caused by MSTIDs, and made two-dimensional maps of the detrended TEC with a spatial resolution of $0.15° \times 0.15°$ in longitude and latitude. MSTID activity is defined as a ratio $\delta I \; / \; \bar{I} \times 100$ [%], where δI is standard deviation of the TEC perturbations within an area of 33.75-37.80^{o} N and 137.50-141.55^{o} E within one hour, and $\bar{I}$ is the background TEC within the same area and period of the corresponding δI.

3. Results: Figure (1) shows the day-to-day variations of the nighttime MSTID activity in summer are compared with that of the Es-layer parameters (foEs and $foEs - fbEs$ ($\equiv$ D$f(o-b)$) obtained at Kokubunji, Japan. We have found that Cross-correlation coefficient between the MSTID activity and $foEs$ (D$f(o-b)$ is larger than 0.3 (0.2) for a period from 1998 to 2019 and figure (2) shows $foEs$ and $Df(o-b)$ are linearly increased with MSTID activity (%). Figure (3) shows the cross correlation coefficient follows the F10.7 is new to understand from this study.

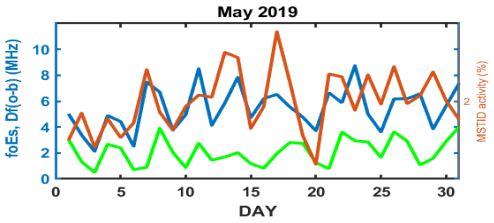

Figure 1. Day-to-day variations of the night time MSTID activity (Red), $foEs$ (Blue) and $Df(o-b)$ (Green)

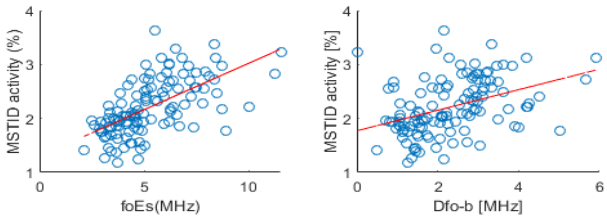

Figure 2. Scatter plot of the night time averages of $foEs$, $Df(o-b)$ and MSTID activity for May–August in 2019.

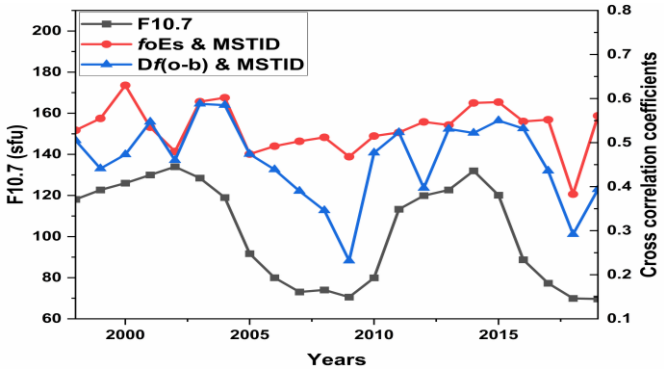

Figure 3. Cross-correlation coefficients and F10.7 during the summer nights of 19-02 hours (JST) of 1998-2019.

4. Conclusion: This result indicates that both MSTID and Es structures could be generated by the electro-dynamical coupling between the Es and F-region through the polarization electric fields. The cross-correlation coefficient tends to increase with solar activity. Considering that the growth rate of the Perkins instability increases with decreasing solar activity, this result suggests that under the high solar activity conditions, when the growth rate of the Perkins instability is relatively low, seeding of polarization electric field perturbations in Es could play a more important role to grow MSTIDs.

5. Period of stay in ISEE: I spent 3 months at ISEE from 04 October 2022 until 27 December 2022.

6. List of publication

Veera Kumar Maheswaran, Yuichi Otsuka, James A. Baskaradas, D. Venkata Ratnam, Sriram subramanian, Atsuki Shinbori, Takuya Sori, Michi Nishioka, Septi Perwitasari. Solar activity dependence for the relationship between nighttime Medium-Scale Traveling Ionospheric Disturbance and Sporadic E-layer activities in summer during 1998-2019 over Japan. (To be submitted)

References:

1. Otsuka et al., (2013) GPS observations of medium-scale traveling ionospheric disturbances over Europe. Ann Geophys.
2. Otsuka et al., (2021) Solar activity dependence of medium-scale traveling ionospheric disturbances using GPS receivers in Japan. Earth, Planets and Space.
3. Perkins F (1973) Spread F and ionospheric currents. J Geophys Res
4. Saito A, Miyazaki S, Fukao S (1998) High resolution mapping of TEC perturbations with the GSI GPS network over Japan. Geophys Res Lett.
5. Shiokawa et al., (2003) Statistical study of nighttime medium-scale traveling ionospheric disturbances using midlatitude airglow imagers. J Geophys Res.

(Form 11-1)

Statistical study of Large-scale Traveling Ionospheric Disturbances (LSTIDs) during geomagnetic storms.

Chukwuma Anoruo. Department of Physics and Astronomy, University of Nigeria, Nsukka.
PhD student

1. Purpose

Travelling Ionospheric Disturbances (TIDs) are the ionospheric manifestation of internal Atmospheric Gravity Waves (AGWs) and are detected as plasma density fluctuations that propagate through the ionosphere with velocities and amplitudes that could depend on the source. TIDs changes ionospheric electron density distribution, resulting in detrimental effects in radio communication, and applications such as the Global Navigational Satellite System (GNSS). Usually,Large-scale TIDs (LSTIDs) are related to auroral geomagnetic activity and have wavelengths over 1000 km, fluctuate at periods from 50 min to 3 h, and have horizontal velocities between 400 and 1000 m/s. Unfortunately, with the few and sparse available ionospheric observatories, it is difficult to observe LSTIDs. This project aims to expand the understanding of the dominant global-energy distribution and momentum transfer mechanisms in the ionosphere and thermosphere due to LSTIDs, and mitigate the detrimental effects in applications and systems that rely on models based on predictions of ionospheric radio-wave propagation physics.

2. Data and Methods

We investigate 49 geomagnetic intense storms occurred between 2004 and 2021, focusing on detecting LSTIDs. In order to study LSTID features, we employ a threshold criteria for amplitude oscillation > 0.1 TECU [1 TECU ~ 10^16 e/m^2], horizontal wavelength > 1000 Km, period of oscillation > 30 min, and horizontal phase velocity > 300 m/s. Ionospheric Total electron Content (TEC) data analyzed in this study is derived from GEONET (https://stdb2.isee.nagoya-u.ac.jp/GPS/GPS-TEC/index.html), a dense wide-area GNSS network in Japan. To obtain the LSTID perturbation signals of TEC (dTEC), 1-hr running average was subtracted from the original time series. Slant TEC is calculated from the GNSS data along the signal path between satellite and GNSS receiver, where phase ambiguity and satellite/receiver biases are ignored. The data for each pair of satellites and receivers is converted from slant to vertical TEC. To determine the horizontal phase velocity and propagation direction of LSTIDs, we employ TEC as function of time and horizontal distance in the meridional and zonal directions (keogram), and considering time series of global dTEC maps at 5 min intervals.

3. Results

Figure 1 shows the global dTEC map for the storm of 17-18March 2015. We observe LSTIDs appear from 14 h UT until 20 h UT on 17 March in the American sector, showing a time difference in the Brazilian sector.

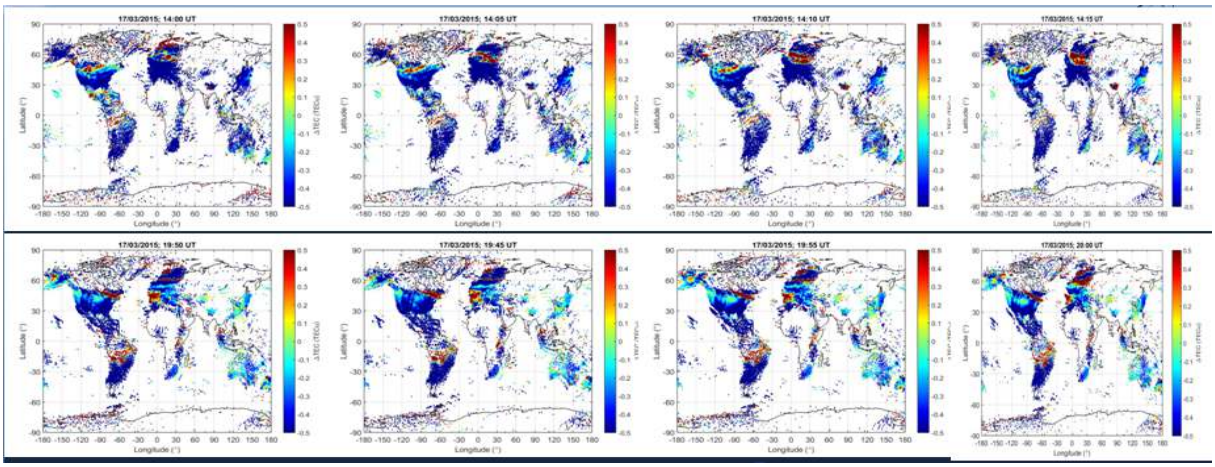

Figure 1. LSTID global dTEC propagations for 17-18, March 2015 geomagnetic storm

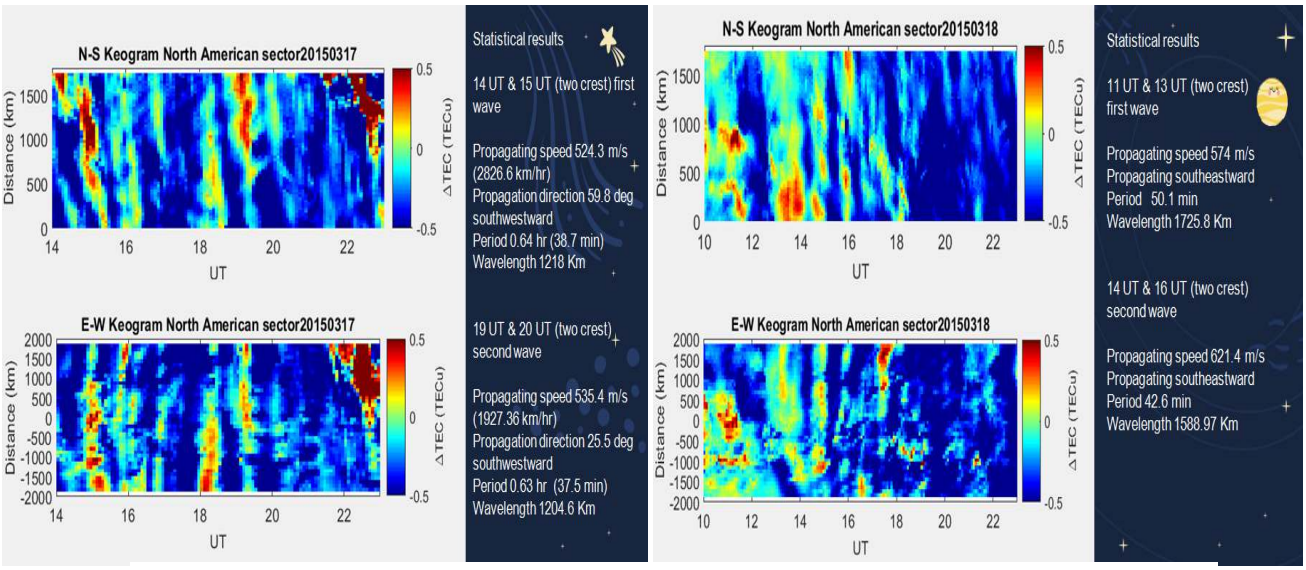

Figure 2. Statistical results of zonal and meridional keogram for March 17-18 LSTID

Figure 2 shows the zonal and meriodional propagation of LSTIDs as a function of time. TEC enhnacements were > 0.2 TECU. At 14 hand15 h UT (two crest), first wave propagates southwest with speed of 524 m/s and with wavelength of 1218 Km.

4. Conclusions

The novelty and advantage of this methodology is to provide high-resolution TEC variations at a global scale.

5. Period of stay in ISEE

3 months, from 17 November 2022 to16 February 2023.

6. List of publication

Anoruo, C.M., Otsuka, Y. et al. Statistical observations of large-scale traveling ionospheric disturbances during the 2015 intense geomagnetic storms [in elaboration]

7. Future works

The characterization of ionosphere irregularities using multiple-source data.

(Form 11-1)

Investigation of Flux Enhancement and associated changes in pitch angle distributions of Radiation Belt particles

Name: Pankaj Kumar Soni
Affiliation: Indian Institute of Geomagnetism, Mumbai, India.
Position: Research Scholar

Principal Investigator Name: Prof. Yoshizumi Miyoshi
Affiliation: Director, Center for Integrated Data Sceince, Institute for Space-Earth Environmental Res earch, Nagoya University
Position: Professor

Objective: To understand the variation in flux enhancement and its effects on the pitch angle distribution of the Radiation Belt particles under different solar wind conditions through satellite observations and their comparison with test-particle simulations.

Earth's magnetosphere operates as a highly efficient particle accelerator driven by inward radial diffusion from higher to lower radial distances, local wave-particle interactions with various magnetospheric waves, or a combination of both processes. In the Earth's magnetosphere, the trapped particles (electrons and ions), consisting of relativistic and ultra-relativistic energies, are located in the inner and outer radiation belt. The motion of these trapped particles is affected by the varying magnetic field, wave-particle interaction, and various types of plasma processes observed by satellites on different spatial and temporal scales. Therefore, radiation belt electrons exhibit highly fluctuating dynamics in their flux and pitch-angle distributions. To comprehensively understand the underlying physical processes responsible for the complex radiation belt electron dynamics, a useful approach is to investigate the evolution of electron pitch angle distribution. This is because electrons of different energies at different pitch angles respond differently to external influences. Therefore, pitch-angle distributions can provide important information on a specific region's source and loss processes. Satellite observations in the Earth's radiation belt regions have reported several distinct shapes of pitch angle distribution. Three commonly observed pitch-angle distributions are pancake, flattop, and butterfly, and are attributed to different physical processes. The pancake distribution has a maximum at ninety degree and minima on both sides. This is the most common type of distribution observed in the dayside inner magnetosphere for the electrons of energies (~ keV), and it is associated with inward radial diffusion. On the other hand, the butterfly distribution has a minimum around ninety degree and a maximum situated on both sides before limiting the loss cone angle. Generally, the butterfly distribution is more common on the night side during 2000- 0400 magnetic local time at higher L-shells. The flattop distribution is characterized by approximately equal flux at most of the pitch angles. Usually, this distribution can be seen as a transitional stage between a pancake and butterfly distribution. It is suggested that the wave-particle interactions during the recovery phase of the geomagnetic storm may result in such flattop distribution.

The geomagnetic storm causes high variability in the dynamics of a magnetospheric particle. Particle fluxes in the radiation belt can be enhanced or depleted following a geomagnetic storm. The change in the particle flux also differs for each phase of the geomagnetic storm. The change in the particle flux leads to the change in the pitch angle distribution depending on the driven source, L-value, energy, magnetic local time, etc. If the particle pitch angle falls into the loss cone, they are no longer trapped and precipitates into the ionosphere via wave-particle interaction. For example, the

interaction of magnetospheric particles with upper and lower band chorus waves accounts for the most intense inner magnetospheric electron diffuse auroral precipitation on the nightside. Therefore, a comprehensive statistical analysis of electron pitch-angle distribution of radiation belt particles for various geomagnetic storms, their storm-time evolution, effect of storm drivers (CMEs/CIRs), effect of wave-particle interaction, and their correlation with atmospheric precipitation are important aspects of radiation belt dynamics.

Arase, formerly known as Exploration of energization and Radiation in Geospace (ERG), operated by ISEE, Nagoya University are dedicated to studying the radiation belt dynamics. We utilized ERG (Arase) data for March 2017 to December 2021, to understand particle flux enhancement, changes in the pitch angle distributions. First, we have selected the geomagnetic storms during the mentioned period with SYM-H less than 40 nT. The pitch-angle resolved data of electron flux from HEP instrument is analyzed of each geomagnetic storm. The particle flux data is obtained for channel 3 to 14 of HEP instrument.

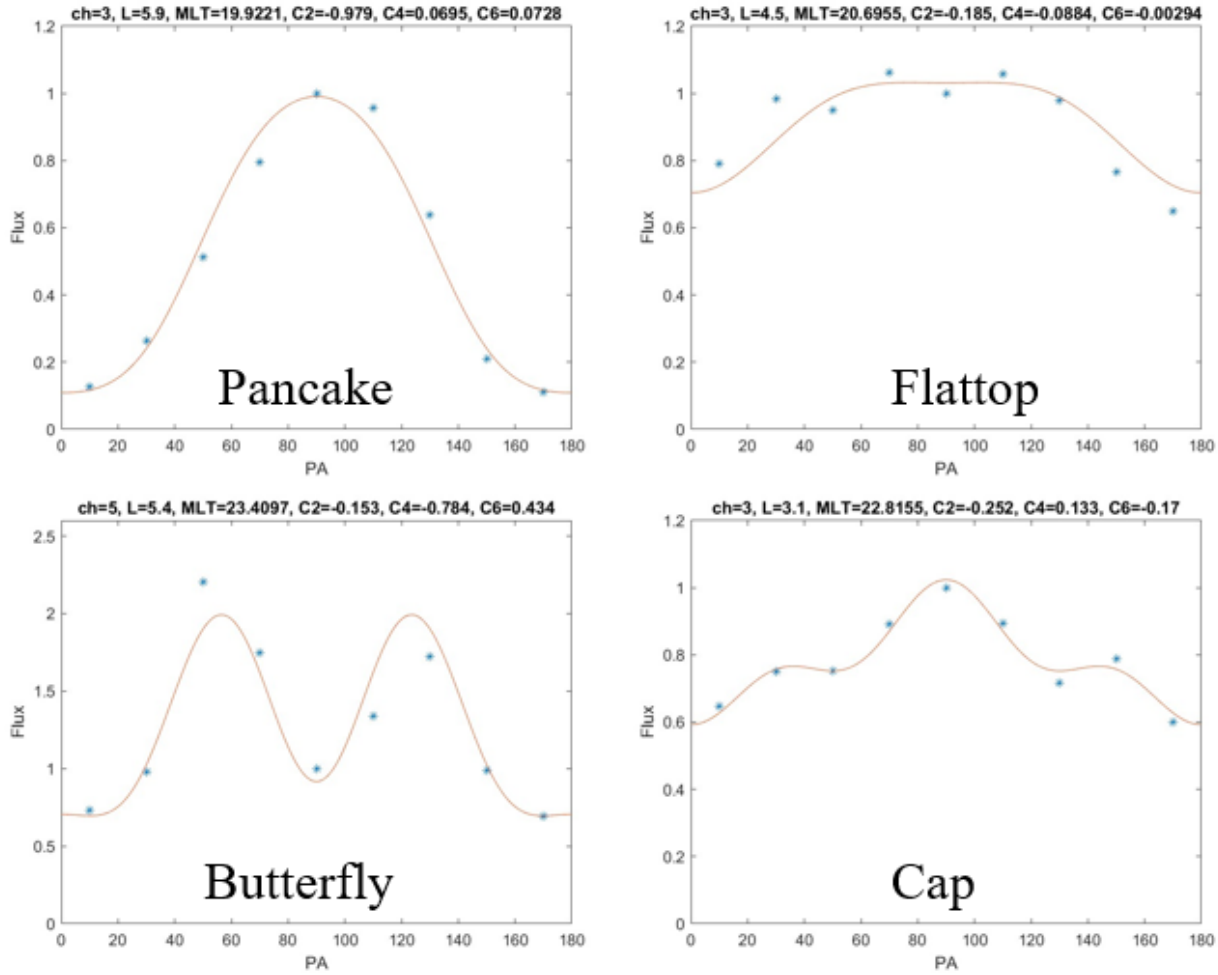

$$C1 = 0;\ C3 = 0;\ C5 = 0;\ \mathbf{C0 \neq 0;\ C2 \neq 0;\ C4 \neq 0;\ C6 \neq 0}$$

The obtained data is separated for in four L-shells (3 to 7) and 12 magnetic local time (MLT) sectors (0 to 24). The pitch angle distribution is obtained for the separated data and fitted with Legendre polynomials up to the sixth degree. The accuracy of fitted pitch angle distribution is checked with root mean square deviation (RMSD). Fitted pitch angle distribution with RMSD larger 0.5 is removed from the statistical analysis. Based on the analysis, L-MLT dependence of particular type of pitch angle distribution is obtained.

Periods of stay in ISEE: October, 5 to December, 20, 2022.

Study of Mesospheric Bores from middle and high latitude region.

Principal Investigator: **Nilesh Chauhan**

Affiliation: **Indian Institute of Geomagnetism, Navi Mumbai, India**

Position: **Senior Research Fellow**

I visited ISEE, Nagoya under the SCOSTEP Visiting Scholars (SVS) program for the duration of 3 months from November 2022 to January 2023. I worked with Prof. Kazuo Shiokawa of ISEE and carried out observational studies on the Mesospheric Tidal Bore structures using the OMTI instruments network of ISEE.

The purpose of the study was to understand the dynamics of mesospheric bore, such as 1) its generation mechanism, 2) propagation characteristics of bores and their seasonal dependence structures. It is also important to study the background environment at the time of the occurrence of mesospheric bores to understand their behavior and propagation through varying medium.

We used high resolution data obtained from the Optical Mesosphere and Thermosphere Imagers (OMTI) network of ISEE, Japan. Five years of data from 2011 to 2015 obtained from the high latitude site, Tromso, Norway and the mid latitude site, Rikubetsu, Japan, were analyzed. The images obtained using optical filters such as OH, Na (589.3 nm), and OI (557.7nm) were studied to identify the mesospheric bore events. In order to obtain information on the background environment during the occurrence of these events, temperature measurements from SABER/TIMED satellite and Sodium Lidar and wind measurements from co-located MF radar site at Tromso were also used. Apart from these datasets we also utilized the reanalysis datasets and satellite-based data, which are essential for this study.

The image data were processed using IDL routines from SPEADAS. We analyzed images with clear sky condition and neglected those images contaminated with auroral activity. We could identify 10 mesospheric bore events from five years of imager data from Tromso observation site. We applied the 3D spectral analysis method (M-transform) developed by Matsuda et al., (2014) to the 557.7 nm emission images to obtain the phase speed of the observed bore events, which turn out to be $\sim$75 m/s. The wavelength and direction of propagation were obtained by visual inspection of the sequence of images.

An example of the mesospheric bore event observed on 24 February 2011 is shown in Figure 1. The event was observed in all three airglow emissions, namely, OH, Na 589.3 nm and 557.7 nm. The bore front was followed by a series of wave-trains behind it. Atleast three waves can be seen behind the bore front. The event was observed for approximately two hours after which the bore appeared to dissipate into the background.

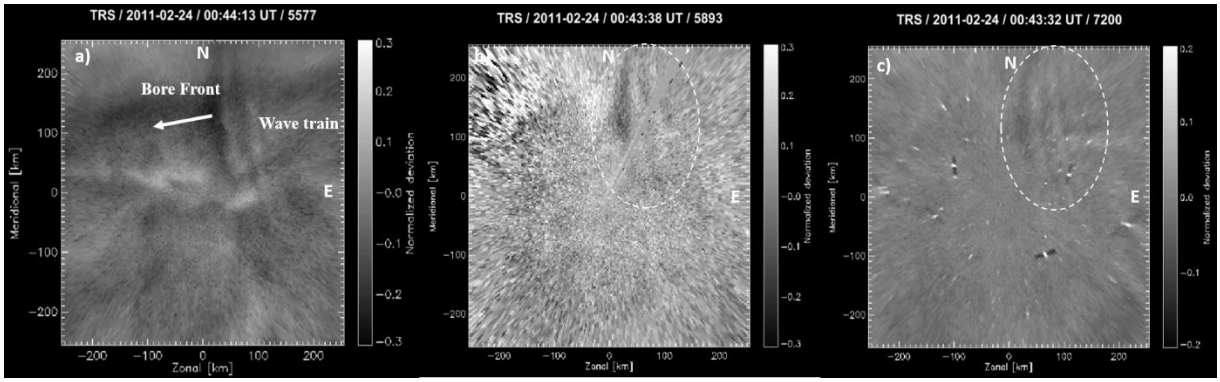

Figure 1: Mesospheric bore observed using airglow emissions: a) OI 557.7 nm b) Na 589.3 nm and c) OH emission images on the night of 24 February 2011. The arrow indicates the direction of propagation of bore front.

Presently, further analysis of wind and temperature data is being carried out by using ground and satellite based instruments. This will help us to obtain a deeper understanding of the dynamics of the mesospheric bore. During my stay at ISEE, I also visited the Shigaraki MU Radar Observatory and acquired insights of various instruments and assisted in the installation of an All-sky camera at the observatory. I also attended the 5th ISEE Symposium during 15-17 November 2022. It was a great learning experience at ISEE and I gained valuable knowledge about the newer research techniques and concepts. This visit also gave me an opportunity to engage in fruitful scientific discussions with various researchers at ISEE, which will surely benefit me in my research career ahead.

(Form 11-1)

Detection of MSTIDs and equatorial plasma bubbles in the low and mid latitude regions using low-cost sky imaging cameras (ZWO Camera).

Wellen Rukundo (Research student - Masters in Space Environment)
Egypt Japan University of Science and Technology (EJUST)
P.O. Box 179, New Borg El-Arab City, postal Code 21934, Alexandria, Egypt
wellen.rukundo@ejust.edu.eg
28/3/2023

RE: Research report for my SCOSTEP Visiting Scholars training program at ISSE, Nagoya University from 1st Dec 2022 to 28th Feb 2023.

1. Introduction

I visited ISEE, Nagoya University for a period of three months from 1st Dec 2022 to 28th Feb 2023 under the SVS program and was supervised by Prof. Shiokawa Kazuo. The purpose for the visit was to learn and train in using low-cost sky imaging cameras for detecting mid and low-latitude ionospheric irregularities. This was motivated by a partnership between EJUST and ISEE, Nagoya University that saw EJUST acquiring three low cost all sky imaging cameras (Z003, Z004 and Z005) taking airglow at different wavelengths of 630 nm, 557nm, and OH bands respectively.

2. Purpose of the training.

The purpose of the visit was to get practical and hands-on skills and learn how to use the cameras for data analysis, visualization, and interpretation in studying the occurrence and properties of MSTIDs and EPBs. And, since ISEE maintains a network of OMTI cameras, this was also an opportunity to do comparative analysis between airglow intensity variation for the low cost and the OMTI camera for improvement of image quality in low-cost cameras.

3. Summary of the results and research output.

We made an analysis of airglow images for the three cameras using a 1hr running averages and observed the gravity wave features in the OH band (Z005) while no such wave features (MSTIDs) were observed in Z003 on day 22/01/2022 at Shigaraki station. The results were consistent with the OMTI camera images at the same station. Then we also compared the airglow intensity variation at the center pixel for each of the three cameras with the photometer of the corresponding wavelength. We found out that the absolute intensity of low-cost cameras is not an accurate measurement due to failure to correct for background intensity in these low-cost cameras which is a limitation for their use in further studying the properties of these mesospheric and thermospheric wave features. However, their trend of airglow intensity variation in raw images is consistent with the trend of calculated intensity in comparison with the photometer hence sufficient to be used to study the occurrence patterns and propagation directions of

these wave features. In other results, we used the Z007 camera (OH band) and studied the occurrence rate of gravity waves at Shigaraki. We noted that about 95% of clear nights showed gravity wave features during the observation period.

From the above results, a first paper describing the basic operation, calibration, and data analysis procedures for the ZWO cameras is being prepared and this will the guiding paper for the new centers of camera installation mostly in the African region. Additionally, I was able to learn some practical skills of equipment installation and troubleshooting to support the new sites in African region.

Finally, I acknowledge the funding support to cater for my living expenses for the three months at ISEE from the administration in partnership with the Center for International Collaborative Research and the support and guidance from my supervisor Prof. Shiokawa Kazuo and the Secretary, Madam Mai Asakura.

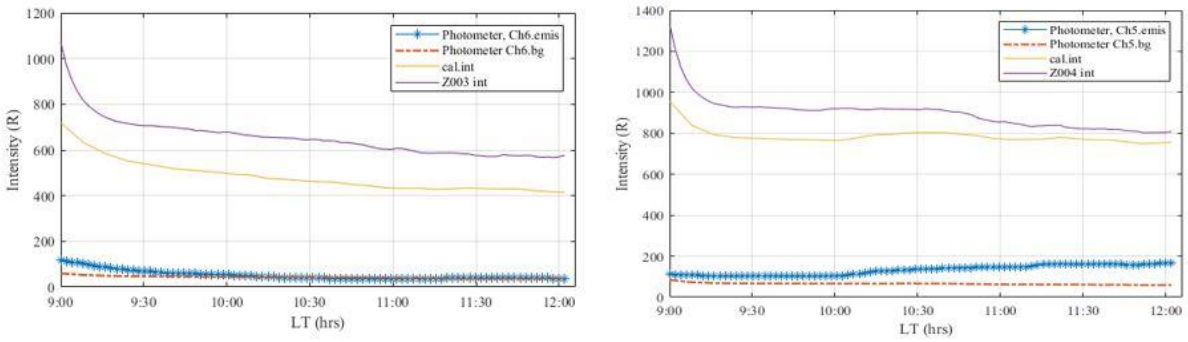

Figure 1: The comparison of ZWO camera and photometer imager at wavelength of 630.0nm filter (left panel) and 557.7nm filter (right panel)

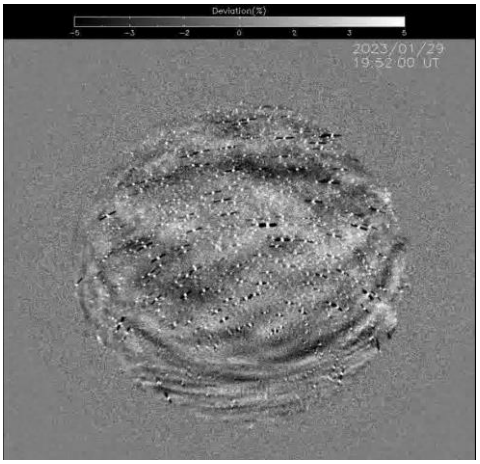

Figure 2: The observation of the gravity wave feature at Shigaraki station on 29/01/2023 by Z007 camera.

Coronal Temperature Variability from Spatially Resolved Images of the Sun from Hinode/XRT

Adithya HN, Scikraft educational and engineering design Pvt.Ltd., Subject Matter Expert(SME)

Purpose of the research:

The outermost atmosphere of the Sun, the corona, extends to several thousand kilometres from the photosphere. It is made up of very tenuous plasma but is very hot. The sudden increase of temperature in the coronal layer from the underlying chromosphere and photosphere makes it very interesting. The average temperature of a corona is measured at about 2 MK, and it may show a large variation in temperature with respect to different surface features. The study of the temperature variation of the full disk of the corona and of individual feature's temperature as a function of the solar cycle will be an interesting

Till now various attempts are made to measure the temperature of coronal XBPs (Kariyappa et. al. 2011) but the temperature of the full disk image and temperature variation of individual features over the solar cycle is not measured yet. Hinode/XRT has a unique feature that using images from two different filters and corresponding filter response curves, the temperature of the sun can be estimated (N. Narukage et. al. 2010).

In this proposed research, using Hinode/XRT data, temperature of the corona and its individual features will be calculated by the filter ratio method from available data sets, for the period of solar cycle 24.

Method implemented:

To study the temperature variability of the solar corona & its features, the full disk level-2 composite data of Hinode/XRT for the period Feb 2008 - Jun 2022 have been downloaded.

The filter ratio method (Narukage et al., 2011, 2014) is used to calculate the temperature of the solar corona. It is one of the unique features of Hinode/XRT. The filter ratio method requires two images from different filters. Since XRT has 8 different diagnostics filters, based on the availability of good data, Al mesh and Ti poly filters were chosen for the period 1st Feb 2008 to 8th May 2012. Ti poly images suffered from stray light leak problem after th May 2012 therefore for the rest of the study Al poly images was used i.e, Al mesh and Al poly image pairs used for the period 9th May 2012 to June 31st 2021.

The filter ratio method assumes that the corona is isothermal. According to the filter ratio method using the ratio of two filter's response functions and the corresponding filter's intensity ratio, The temperature of the corona can be calculated. The response function of the two filters for each image with respect to the thickness of the contamination layer was extracted using IDL/SSW routine 'make xrt temp resp.pro'. According to the filter ratio method for a temperature 'T,' we can write,

$$F_1 / F_2 = I_1 / I_2$$

Where F_1 = Filter response of Ti-poly/Al-poly, F_2 = Filter response of Al-mesh, I_1 = Intensity of Ti-poly/Al-poly image, I_2 = Intensity of Al-mesh image

A sophisticated python algorithm has been developed to generate temperature images by mapping intensity ratio values to corresponding temperature values by referring to the ratio of the filter's response curve vs the temperature value.

By overlaying segmentation maps obtained from our previous study (Adithya et al., 2021) on temperature image the average temperature of the features ARs, CHs, BGs, and XBPs and their contribution to the full disk were extracted and compared with Sunspot numbers.

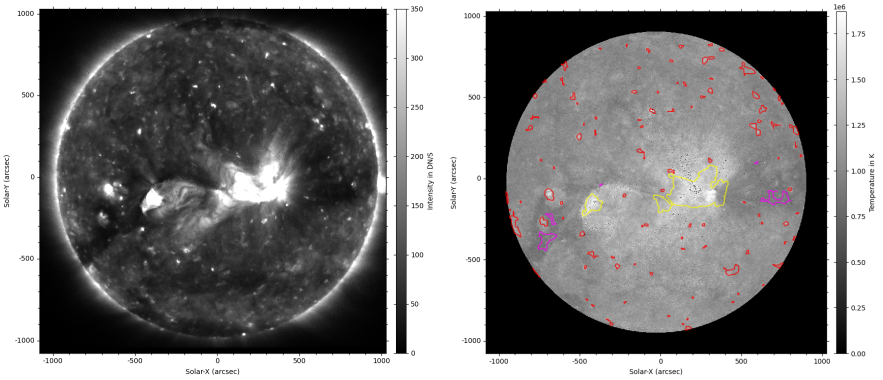

Figure 1: Al mesh intensity image(left), temperature image(right) for the day 4 Feb 2008. Yellow colour contour represent AR, red is XBPs and violet represent CH, remaining is BG

Results

- The average temperature of full disk and other features (ARs, CHs, BGs, & XBPs) estimated for the period Feb 2008 - June 2022.

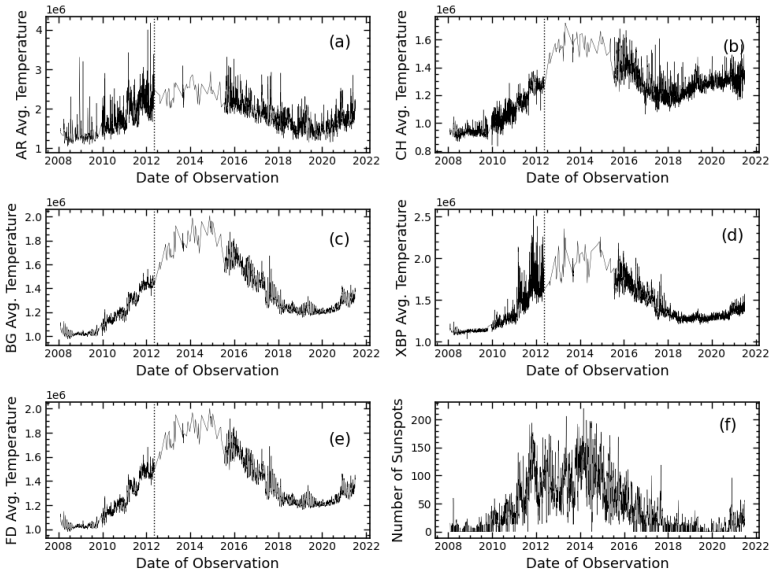

Figure 2: Time series of temperature variation of full disk and all features. Vertical line separates the temperature estimation from Al mesh-Ti poly (left side of vertical line) and Al mesh-Al poly (right side of vertical line)

- Temperature of all the features vary as a function of sunspot number (solar activity).
- The average temperature of the full disk for the period was 1.29 MK and other features such as AR, XBP, CH and BG temperature were 1.76 MK, 1.32 MK,1.23 MK and 1.27 MK respectively.
- The mean temperature contribution for the full disk estimate of background (BG) is 93.18%, whereas ARs, XBPs and CHs are 3.12%, 2.12% and 1.58%. Since the background occupies more area it is the dominant temperature contributor for the full disk.

Period of stay: April 16 2022 to July 15 2022 (3 months)

Publication: H. N. Adithya, R. Kariyappa, Kanya Kusano, Satoshi Masuda, Shinsuke Imada, J.J. Zender, L. Dame, Mark Weber and E. E. DeLuca, 2022, *Solar Soft X-ray Irradiance Variability, II: Temperature Variations of Coronal X-ray Features*, Sol. Phys. (Submitted, under review)

Investigation of the thermospheric wind observations during geomagnetic quiet periods using ground-based and satellite-based data, and model simulation

Nwankwo Onyinye Gift, University of Michigan, 2022 SVS Recipient

Purpose of study

The purpose of this research was to investigate the behavior of thermospheric winds during geomagnetic quiet periods by combining ground-based Tromso Fabry-Perot Interferometer (FPI) data and CHAMP satellite data with model simulations using the Global Ionosphere Thermosphere Model (GITM). By studying the thermospheric winds during periods of low geomagnetic activity, the research aimed to enhance our understanding of the dynamics of the Earth's upper atmosphere and the role of the magnetosphere in driving these dynamics. The findings of this study have the potential to improve our ability to model and predict space weather and its impacts on space-based technologies and communication systems.

Methodology

We investigated the dynamics of the upper atmosphere through nocturnal airglow emissions using the Optical Mesosphere Thermosphere Imagers (OMTI) Tromso FPI data and International Monitor for Auroral Geomagnetic Effects (IMAGE) magnetometer data. To obtain the X North component (nT) of the magnetic field in the region of interest, we accessed IMAGE magnetometer data from https://space.fmi.fi/image/www/index.php?page=user_defined. The Tromso site where the data was obtained is located at a high latitude region with a geographic (geomagnetic) latitude of 69.58°N (66.73°N). To define the quiet periods for the investigation, we used the quiet periods outlined in Table 1 by Heqiucen et al., (2019).

Next, we used the Tromso FPI data to provide us with measurements of the neutral wind velocity in the thermosphere, as well as observations of the dynamics of the upper atmosphere through the analysis of the airglow emissions. We conducted two runs of the Global Ionosphere-Thermosphere Model (GITM) using two aurora drivers: Fuller-Rowell & Evans (FRE) and Feature Tracking Aurora (FTA) models, to simulate the behavior of the upper atmosphere based on the data obtained from the IMAGE magnetometer and OMTI Tromso FPI observations. The outputs from the simulations allowed us to further investigate the dynamics of the upper atmosphere during the nocturnal period.

Results

Figure 1 shows the quiet-time average winds in the thermosphere in the zonal and meridional directions, as well as the X North component (nT) and AE (nT) index for February 16th 17:07 UT (18:07 LT) through 17th 04:19 UT (05:19 LT). the zonal wind started with a westward flow, and reversed to eastward flow with peak values reaching over 100 m/s at around 20 UT (21 LT). This is typical of wind driven by plasma convection. However, the winds in the meridional directions did not show much variability, had southward flow with peak reaching 200 m/s at around 22 LT. The X North component of the magnetic field (nT) exhibited high variability till at about 23 LT, it showed relatively stable values throughout the remaining time period. This variability in the X North component of the magnetic field (nT) until around 23 LT may have been due to fluctuations in the Earth's magnetic field or the effects of solar activity on the upper atmosphere. The AE index shows a slight increase in activity during the observation period, with peak values reaching just over 250 nT. The reversal to the eastward flow at around 21 LT may have been caused by a sudden reversal in the direction of the plasma convection, while the relatively stable winds in the meridional direction may have been due to the lack of strong atmospheric tides or wave activity in that direction, which can have implications for the transport of heat and momentum in the upper atmosphere.

Figure 2 shows the descending node plots for CHAMP zonal wind and GITM zonal wind. In the equatorial to mid-latitude regions, both data and model shows eastward flow, while at high latitude, they show westward flow. The westward flow observed in both the CHAMP zonal wind and GITM zonal wind in the high-latitude regions may be due to the effects of ion drag, which occurs when the neutral winds in the thermosphere interact with the ionosphere.

Periods of stay in ISEE

September 12th, 2022 through December 10th, 2022

List of publications

1. **Onyinye G. Nwankwo**, Fabio Becker-Guedes and Claudia MN Candido, "Space weather effects on the Brazilian equatorial and low-latitude ionospheric Maximum Usable Frequency (MUF) during the Saint Patrick's Day geomagnetic storm." Poster presentation at CEDAR 2021 Workshop. https://youtu.be/QQ2-8sCEjmI
2. Rachelle Winterberger, Chen Wu, Aaron Ridley and **Onyinye G. Nwankwo**, "Comparisons between TIDI and other Wind measurements." Poster presentation at 2021 AGU Fall meeting.(https://agu2021fallmeeting-agu.ipostersessions.com/default.aspx?s=30-25-BC-82-6A-6F-D8-F8-6F-A1-2D-5B-4B-6D-0E-F6)
3. **Onyinye G. Nwankwo**, and Aaron J. Ridley, Storm and Non-storm time thermosphere and ionosphere, Presentation Talk at CEDAR Workshop, Austin, Texas, June 19-24, 2022
4. **Onyinye G. Nwankwo**, and Aaron J. Ridley, Investigating the impact of geomagnetic storm over the ionosphere-thermosphere system of subauroral/midlatitude region using ISR observations and GOCE measurements, Poster presentation at CEDAR Workshop -June 2022
5. Aliaa A. M. Afify, **Onyinye G. Nwankwo**, and Aaron J. Ridley, Solar EUV Driven Radiative Transfer in the Thermosphere: Modeled using Runge Kutta 4th Order Method, Presentation Talk at ICELLI Workshop -September 2022
6. **Onyinye G. Nwankwo**, Aaron J. Ridley, and Kazuo Shiokawa, Quiet-time Variation of the Horizontal Neutral Wind at High Latitude using CHAMP data, FPI measurements and GITM simulation, Presentation Talk at the Space Science Seminar Series, University of Michigan -October 2022
7. **Onyinye G. Nwankwo**, Aaron J. Ridley, and Kazuo Shiokawa, Global variation of quiet-time Zonal Wind using GOCE and CHAMP satellite data, and GITM simulation, Presentation Talk at the 12th National Annual Conference of the Astronomical Society of Nigeria (ASN) -November 2022

8. **Onyinye G. Nwankwo**, and Aaron J. Ridley, Exploring the ion-neutral electrodynamics of mid-latitude upper atmosphere: Insights from GITM simulation, Madrigal TEC, and Fabry-Perot interferometer data for March 2013 Storm, Presentation Talk at the Space Science Seminar Series, University of Michigan -March 2023
9. **Onyinye G. Nwankwo**, and Aaron J. Ridley, Investigating ion-neutral dynamics of Mid-Latitude Upper Atmosphere with GITM Simulation, Madrigal TEC and Fabry-Perot Interferometer Data, Poster presentation at Space Weather with Quantified Uncertainties (SWQU) Spring Meeting, MIT, Boston -March 9-10, 2023

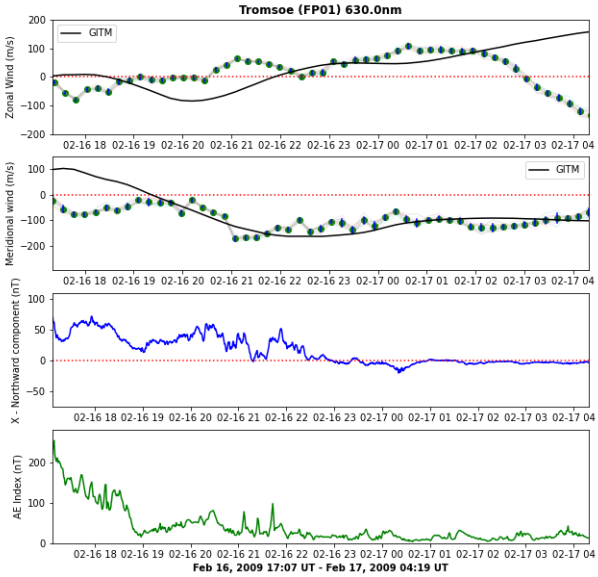

Figure 1 shows the quiet-time average winds in the thermosphere in the zonal and meridional directions, X North component (nT), and AE (nT) index for February 16th 17:07 UT (18:07 LT) through 17th 04:19 UT (05:19 LT). The LT conversion is because Tromso, Norway's local time (LT) is 1 h ahead of universal time (UT).

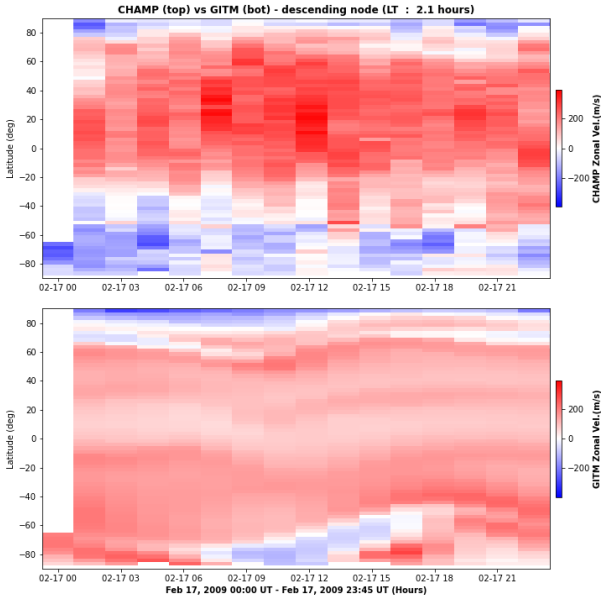

Figure 2 shows the descending node plots for CHAMP zonal wind and GITM zonal wind.